Supporting Information

Soe-Lin et al. 10.1073/pnas.0900808106

SI Results

Determination of Nonheme Iron. Quantification of liver and splenic nonheme iron was carried out according to the method of Pountney et al. (1). Briefly, liver and spleen tissues were homogenized in 700-μl iron-free distilled water by using a Kontes pestle (Fisher Scientific). The homogenate was then boiled in 20-μl 12N HCl for 10 min, after which 200-μl 50% trichloroacetic acid was added, and the samples were cooled on ice for 15 min. Precipitated protein was then spun down by centrifugation (21,000 $\times$ *g*/15 min) and supernatants were collected into separate tubes. After collection, 40-μl 10 M NaOH was added to each supernatant. The nonheme iron content was determined by the addition of ferrozine reagent (0.88-g ascorbate, 4.3-g sodium-acetate, and 98-mg ferrozine in 50-ml iron-free water) to each sample. The absorbance at 562 nm was determined and compared against a standard curve of $FeCl_3$. Nonheme iron was standardized to tissue wet weight, and is expressed as μg Fe/g wet weight.

Organ Pathology and Tissue Iron. The spleen index was expressed as a ratio of spleen weight to total body weight. To visualize pathological iron deposits, Perls' Prussian blue staining was performed on liver and spleen sections as previously described (2). Spleens and livers were fixed in 10% phosphate-buffered formalin overnight and then were embedded in paraffin blocks. The 4-μm sections were stained with hematoxylin and eosin. Tissues were scored for blue-positive iron deposits at 40$\times$ magnification by using a Zeiss Axiophot image analysis microscope. Three representative nonoverlapping fields were examined for each organ. Areas staining positive for iron were converted to pixels and were expressed as a percentage of total surface area of the field by using Northern Eclipse 6.0. The percentages of stainable areas from each sample were averaged.

RNA Isolation, cDNA Synthesis and Quantitative Real-Time RT-PCR. Total RNA was isolated from liver samples by using TRIzol reagent (Invitrogen), including treatment with DNase to eliminate possible genomic DNA contamination. cDNA was isolated from 5–10 μg of RNA by using a first-strand synthesis kit (Invitrogen) with Moloney murine leukemia virus reverse transcriptase and oligo(dT) in a 20-μl reaction volume. Quantitative real time RT-PCR was performed by using a Light-Cycler apparatus (Roche Diagnostics) and SYBR Green I fluorescent dye (Molecular Probes). β-actin was used as an internal control for normalization. The primers used for hepcidin and β-actin were: Hepcidin forward, 5′ATGGCACTGAGCTCCCAGAT-3′; hepcidin reverse, 5′-ACTTTGATCGATG-ACAGCAGCCG-3′; β-actin forward, 5′-AGGATGCAGAAGGAGATCACT-3′; and β-actin reverse, 5′-GGGTGTAACGCAACTAAGTCATAG-3′.

Flow Cytometry Analysis of Splenic Erythroblasts. Both Nramp1$^{+/+}$ and Nramp1$^{-/-}$ mice experienced dramatic splenomegaly because of extramedullary erythropoiesis after acute and chronic phenylhydrazine treatment. We sought to further characterize the erythroblasts contained within the spleens to determine whether impaired macrophage iron release affected erythroid cell differentiation and maturation. The splenic erythroid population from untreated Nramp1$^{+/+}$ and Nramp1$^{-/-}$ mice is shown in Fig. S3. After acute phenylhydrazine treatment, there was an increased shift of the erythroid progenitors toward the basophilic (CD71high/Ter119high) and orthochromic (CD71low/Ter119 high) populations as a result of stress erythropoiesis in both WT (Fig. S3*C*) and KO (Fig. S3*D*) animals. With chronic administration of phenylhydrazine, there was a mild impairment of erythroid differentiation in the spleens of Nramp1$^{-/-}$ animals (Fig. S3*F*) with increased basophilic (quadrant III) and reduced orthochromatic (quadrant IV) erythroblast populations as compared with Nramp1$^{+/+}$ mice (Fig. S3*E*), although this discrepancy was not statistically significant. This slight block in erythroid differentiation in Nramp1$^{-/-}$ splenic erythroblasts, however, was consistent with the reduced hematocrit observed in the Nramp1$^{-/-}$ mice after chronic phenylhydrazine treatment.

1. Pountney DJ, et al. (1999) Iron proteins of duodenal enterocytes isolated from mice with genetically and experimentally altered iron metabolism. *Br J Haematol* 105:1066–1073.

2. Szuber N, et al. (2008) Alternative treatment paradigm for thalassemia using iron chelators. *Exp Hematol* 36:773–785.

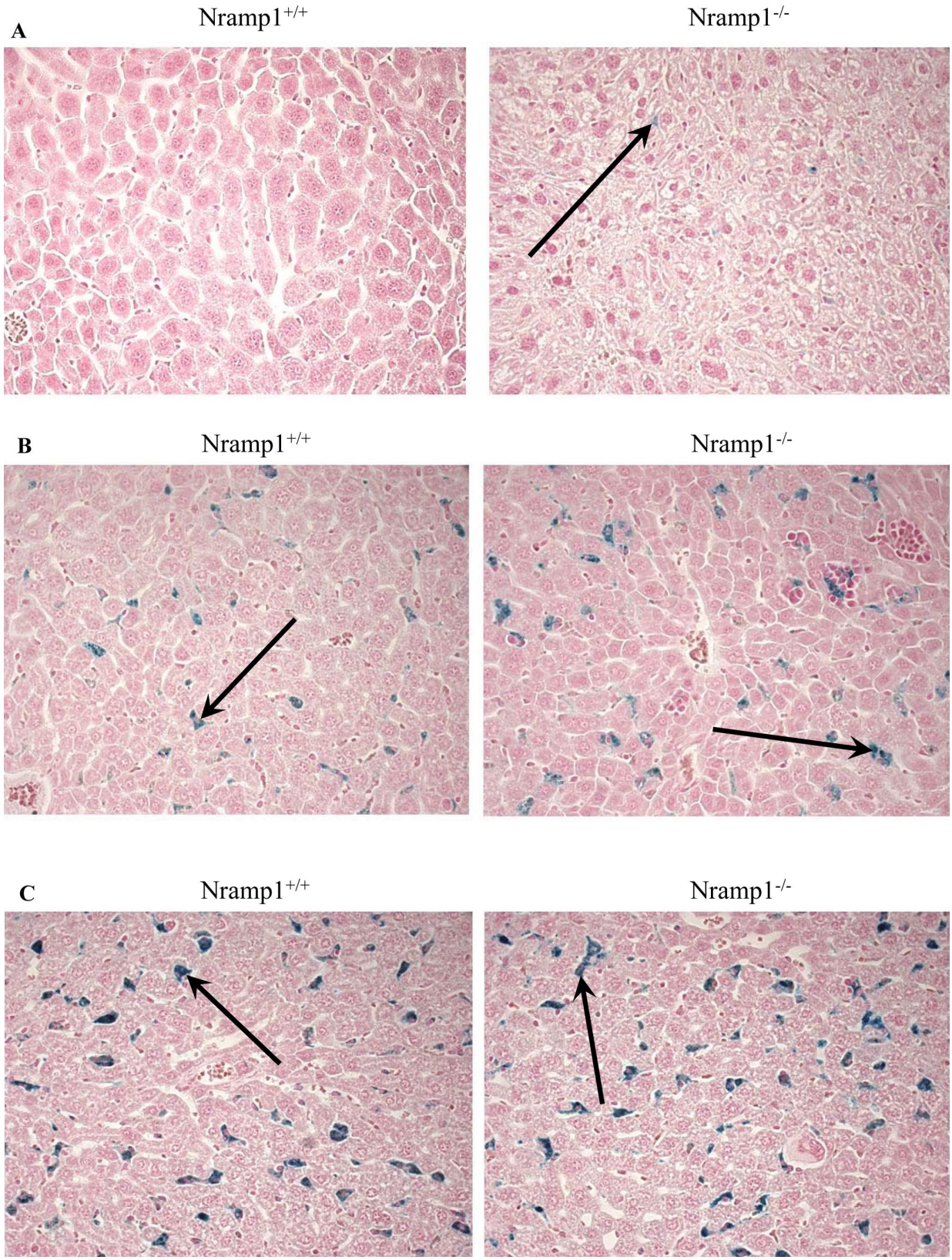

Fig. S1. Perls' Prussian blue staining was performed to visualize the location of iron deposits within the liver of untreated 5-week-old mice (*A*), acute-treated mice (*B*), and chronically treated mice (*C*).

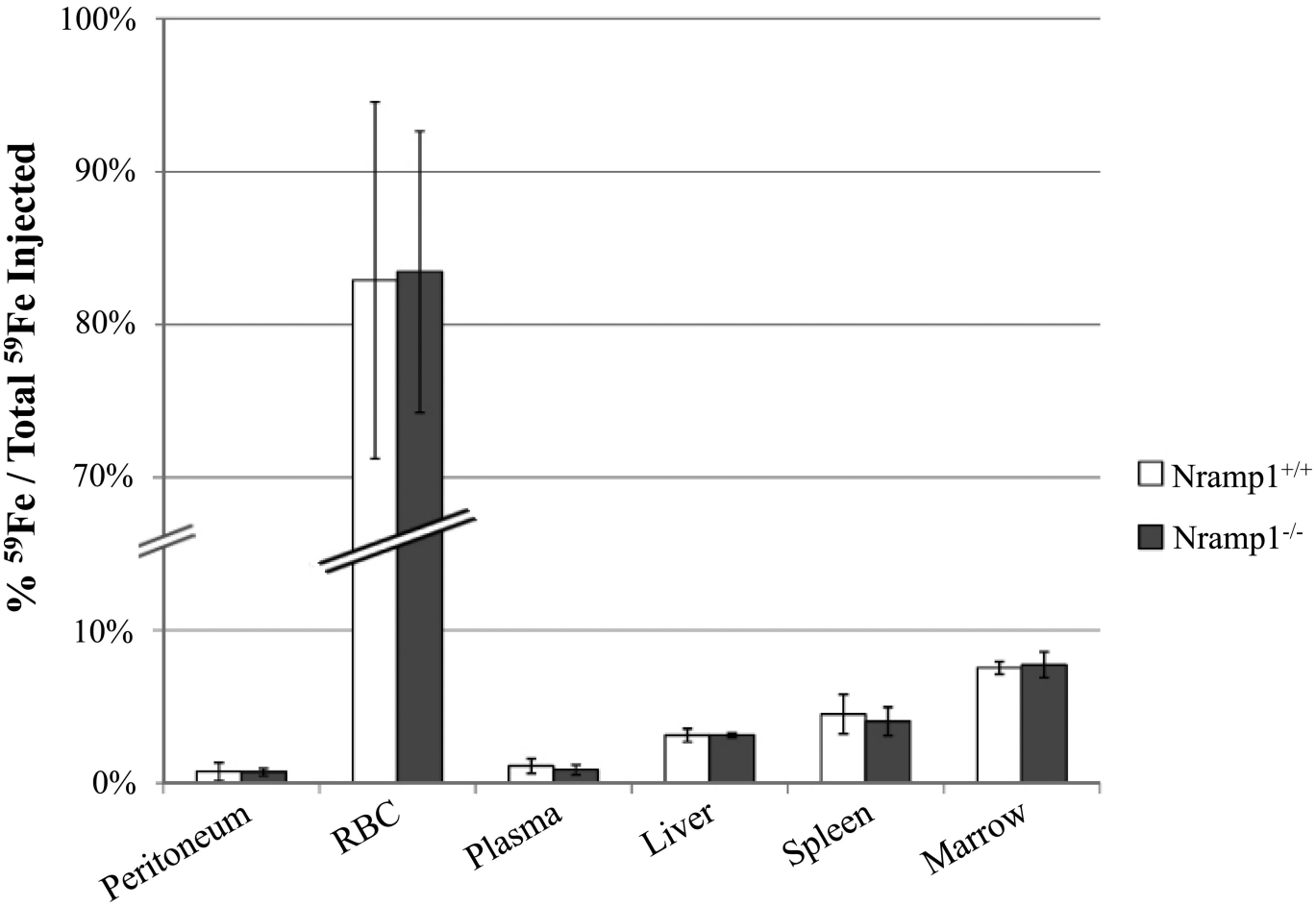

Fig. S2. Both WT and KO mice are equally able to absorb 59Fe-transferrin injected i.p. and to incorporate ^{59}Fe within new circulating erythrocytes. Mice were injected with 200 μl of 0.25 μM ^{59}Fe-transferrin i.p., and the incorporation of ^{59}Fe within each bodily compartment was assessed 24 h later. At least 3 animals were used for each group.

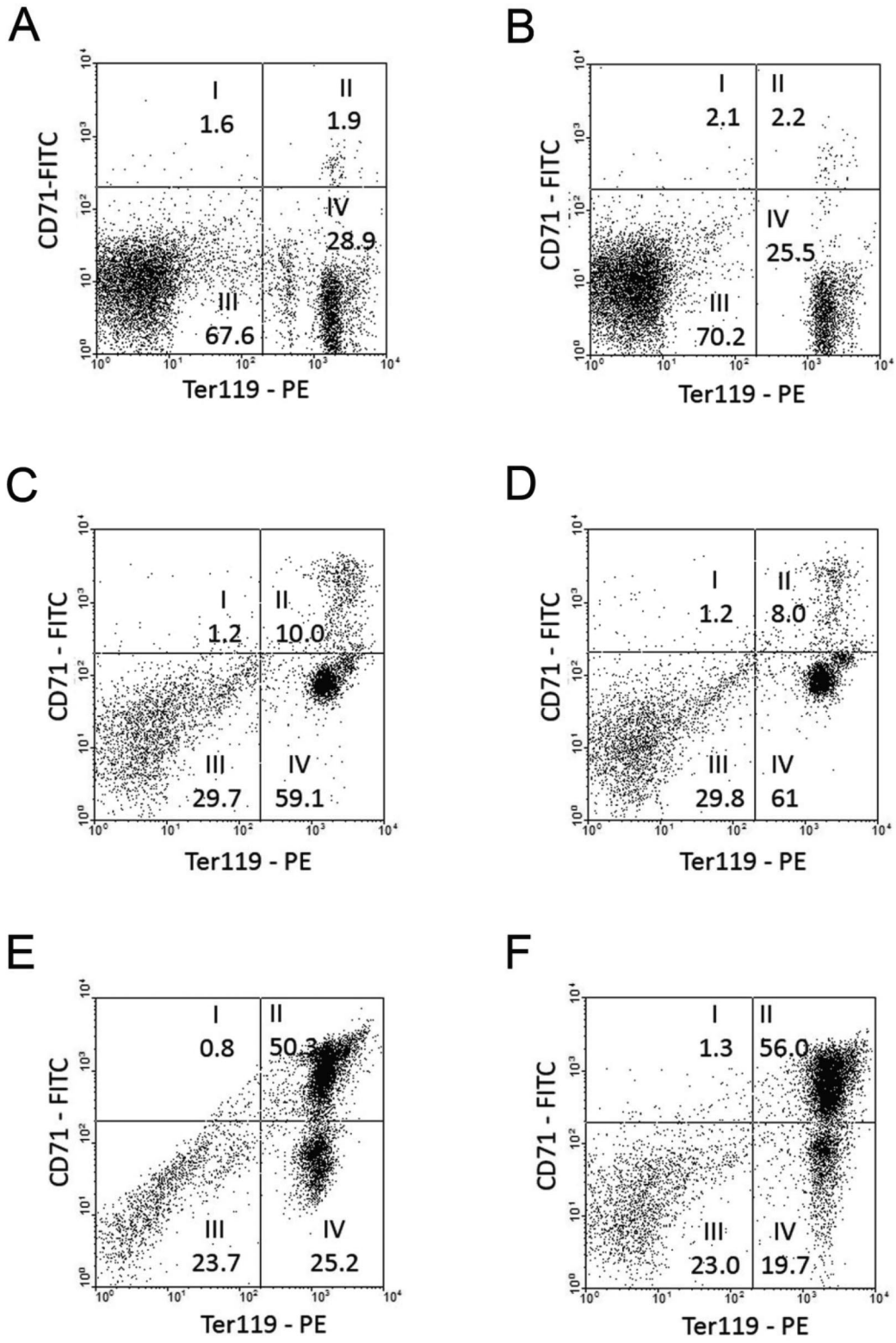

Fig. S3. FACS analysis of splenic erythroblasts from untreated, acute, and chronically treated mice. Representative flow cytometric analyses of splenic erythroblasts from WT and KO mice were immunostained with antibodies to CD71 (transferrin receptor) and Ter119. The relative percentages of all viable, nucleated cells in each of the quadrants are indicated. (*A*) WT, untreated; (*B*) KO, untreated; (*C*) WT, acute hemolytic anemia; (*D*) KO, acute hemolytic anemia; (*E*) WT, chronic hemolytic anemia; (*F*) KO, chronic hemolytic anemia. All animals used were 5 weeks old.